



HAL
open science

Assessment of shear-thinning fluids and strategies for enhanced in situ removal of heavy chlorinated compounds-DNAPLs in an anisotropic aquifer

Iheb Bouzid, Nicolas Fatin-Rouge

► **To cite this version:**

Iheb Bouzid, Nicolas Fatin-Rouge. Assessment of shear-thinning fluids and strategies for enhanced in situ removal of heavy chlorinated compounds-DNAPLs in an anisotropic aquifer. *Journal of Hazardous Materials*, 2022, 432, pp.128703. 10.1016/j.jhazmat.2022.128703 . hal-03842004

HAL Id: hal-03842004

<https://hal.science/hal-03842004>

Submitted on 22 Jul 2024

HAL is a multi-disciplinary open access archive for the deposit and dissemination of scientific research documents, whether they are published or not. The documents may come from teaching and research institutions in France or abroad, or from public or private research centers.

L'archive ouverte pluridisciplinaire **HAL**, est destinée au dépôt et à la diffusion de documents scientifiques de niveau recherche, publiés ou non, émanant des établissements d'enseignement et de recherche français ou étrangers, des laboratoires publics ou privés.



Distributed under a Creative Commons Attribution - NonCommercial 4.0 International License

1 Assessment of shear-thinning fluids and strategies for enhanced *in situ* removal
2 of heavy chlorinated compounds-DNAPLs in an anisotropic aquifer

3 Iheb Bouzid ^a, Nicolas Fatin-Rouge ^{a,b}

4 ^a *Université de Bourgogne Franche-Comté–Besançon, Institut UTINAM–UMR CNRS 6213, 16, route de*
5 *Gray, 25030, Besançon, France*

6 ^b *Institut de Chimie des Milieux et Matériaux de Poitiers (IC2MP), Université de Poitiers, UMR-CNRS*
7 *7285, F-86073 Poitiers, France*

8 Corresponding author : Nicolas Fatin-Rouge

9 Email : nicolas.fatin-rouge@univ-poitiers.fr

10

11 Abstract:

12 The removal of chlorinated organic hydrocarbons (COHs) -DNAPLs was studied in permeability-
13 contrasted sandboxes with an egg-box shaped substratum. Aqueous solutions were compared to
14 viscous shear-thinning fluids (xanthan solution and foam). Interfacial and viscous effects were
15 compared by increasing the capillary number of injected fluids. Non-spatially targeted DNAPL
16 recovery (NSTR) where the driving force was the injection pressure, was compared to spatially
17 targeted DNAPL recovery (STR) where a pumping system allowed the controlled flow. A historical
18 contamination made of a complex mixture of COHs and hexachlorobutadiene (HCBD) as a model
19 were used. NSTR results showed that DNAPL recovery with non-viscous liquids did not exceed 40%.
20 The best results were obtained for xanthan solutions with surfactant $\sim 1.3 \times \text{CMC}$ for which pure
21 phase recovery amounted to 88% and 93% for HCBD and for the historical DNAPL, respectively. The
22 STR strategy showed similar recovery yields, whereas xanthan concentrations were 10-times lower.
23 Mass balances on DNAPL showed that at most, 0.15% of COHs was dissolved in the aqueous
24 effluents. NZVI (1 g.l^{-1}) were delivered in xanthan in view of the chemical degradation of residual
25 COHs and showed a 65% transmission through the low permeability soil.

26

27 Keywords: DNAPL removal; underground anisotropy; xanthan gum; surfactant foam; NZVI

28

29 1. Introduction

30 Chlorinated organic hydrocarbons (COHs) are hazardous and widespread contaminants in soils and
31 groundwater. COHs have been released for decades into the environment because of their use in
32 anthropogenic activities [1,2] and the presence of dense non-aqueous phase liquids (DNAPLs) of
33 COHs in these media results of spillages. These DNAPLs percolate to the aquitard because of their
34 high density and low solubility in water. As the free phase moves downwards, it leaves behind a
35 residual phase as droplets or pools when its capillary pressure is lower than the entry pressure of
36 pores. Pollutants are released in the long term from source zones into groundwater, as large plumes,
37 whose magnitude is connected to their mass, threatening human health and aquatic life [3].

38 Extensive research has been carried out, highlighting the inherent difficulties of removing DNAPLs
39 from heterogeneous aquifers, as their lack of accessibility represents a real challenge for clean-up
40 operations. Pump and treat (PT) and soil flushing (SF) are commonly used for DNAPL treatment, yet
41 they suffer limitations from DNAPL and underground (geological and contamination heterogeneity
42 and anisotropy) characteristics [4]. Typical PT recovery rates do not exceed 60%, even at their highest
43 values [5]. SF enables DNAPL mobilization owing to interfacial tension (IFT) reduction, however, this
44 technology is controversial and scarcely used, because of the risks associated to uncontrolled
45 mobilization [6,7]. Moreover, usual low viscosity liquids used for remediation display fingering and
46 preferential flows through the most permeable pathways, making treatments ineffective [8–10].
47 Consequently, there are still challenges, since many DNAPL-contaminated sites cannot be brought to
48 regulatory criteria within a reasonable time frame, because of the lack of efficient technologies for
49 their removal.

50 Improving the sweeping efficiency and the mobilization ability of flushing fluids for DNAPL-recovery
51 in anisotropic media requires to increase their capillary number [11,12]. This well-known issue led to
52 the use of viscous, but shear-thinning fluids in oil recovery [13–17]. These behaviors, observed for
53 associative polymers like xanthan and for foams, are useful for the *in situ* remediation (ISR) of
54 contaminated underground [4,8,25–29,9,18–24].

55 Within the PAPIRUS project (French acronym for Upwelling Technology and Injection of Stabilizing
56 Agents for Assisted Pumping using Tilted Recovery Wells), the enhanced DNAPL-recovery in a
57 strongly heterogeneous aquifer using viscous injected fluids is studied. A historical DNAPL situated at
58 8-10 m below the ground surface (bgs) is laying onto an egg-box topology clayey substratum. In that
59 challenging situation of low DNAPL accessibility, the controlled propagation of remedial fluids is

60 critical for the achievement of the treatment goals. Here, special care is given to the field
61 applicability of this technology.

62 Several authors showed the efficiency of surfactant foam and polymer solutions for DNAPL recovery
63 in micromodels [30], in columns [4,26,28,31], in sandboxes [7] and in the field in an alluvial aquifer
64 [25]. However, none of the studies was carried out in a complex situation consisting of two
65 permeable layers above a wavy impermeable layer where DNAPL accumulates and sticks to low
66 accessibility interfaces. This situation corresponds to a real recurring type of contamination which
67 represents a technical challenge.

68 In this paper, first, the non-spatially targeted DNAPL recovery (NSTR) was assessed for various water-
69 based fluids whose propagation was only controlled by injection forces. Unique aspects of this work
70 include the comparison of the sweep efficiency of non-dense Newtonian and non-Newtonian fluids
71 to recover the contamination in anisotropic 2D-sandboxes, essentially in the form of a pure phase.
72 Second, spatially targeted DNAPL recovery (STR) was performed after the high permeability layer was
73 blocked. Fluids propagation was assisted by pumping which allowed to induce their converging flow.
74 Surfactant foams were used in sandboxes and assessed on field as a blocking agent. The latter was
75 formed in the most permeable horizon to divert a surfactant solution to a less permeable horizon
76 where the DNAPL was [32,33]. The approach developed in our study is different since both surfactant
77 foam and polymer solutions were evaluated in anisotropic sandboxes as blocking agents in an
78 injection/pumping setup. Martel [34,35] assessed at pilot and field scales, an injection-pumping
79 pattern involving the use of polymer solutions to control the mobility of a washing solution slug for a
80 DNAPL recovery. The authors reported a complete sweep of the remediated area, but tests were
81 performed in overall isotropic sand without DNAPL pits. To the best of our knowledge, no studies
82 were carried out within the overall framework of a performance comparison between blocking and
83 mobilization strategies for DNAPL recovery. No systematic quantitative analysis of fluids numbers
84 was performed either. Finally, after the controlled DNAPL recovery phase was achieved, the injection
85 of zero-valent iron nanoparticles (NZVI) in columns and sandboxes was studied. It allowed the *in situ*
86 creation of a reactive NZVI-barrier to complete the removal of residual contaminants through
87 dehalogenation reactions [36]. Previous studies have reported the use of NZVI to degrade COHs [37–
88 40]. Here, hydraulics control for NZVI delivery following pure phase recovery is of main importance
89 for the success of the polishing treatment.

90

91 2. Materials and methods

92 2.1. Soils and DNAPL

93 The solid materials were chosen to mimic the complex lithology of the contaminated site located in
94 France. An accidental leakage of a complex mixture of COHs occurred there in the late 1960s
95 [25,41,42]. A DNAPL of contaminants migrated into the soil, down to the clayey aquitard [4,26]. The
96 main components of the historical DNAPL were hexachlorobutadiene (HCBD, 58%),
97 hexachloroethane (16%), perchloro-ethylene (8%), and pentachlorobenzene (3.5%). Considering the
98 geological characteristics of the site, three layers of different permeabilities were chosen to
99 reproduce the anisotropic aquifer in sandbox experiments (see Fig. 1). From bottom to top, the first
100 layer was an impermeable egg-box shaped clay layer, which represents the substratum of the
101 aquifer. The second one was a low permeable layer (LPL) made of fine glass beads purchased from
102 Sigmund Lindner. The third one was a high permeability layer (HPL) made of glass grains provided by
103 Oré peinture. Model translucent soils were used in this study to allow a good visualization of both
104 the dyed DNAPL and remediation fluids behaviors. The permeabilities, porosities and grain sizes were
105 13 and 130 μm^2 , 44 and 43% and 100-200 and 150-1000 μm for the LPL and the HPL, respectively.
106 Their particle size distribution is shown in figure S1.

107 2.2. Chemicals

108 Xanthan gum ($\geq 99\%$, Rhodicare) was supplied by Solvay in the form of a dry powder and the solution
109 preparation can be found elsewhere [8]. The anionic surfactant sodium dodecylbenzene sulfonate
110 (Technical grade, SDBS, Aldrich, CMC = 0.07%) was selected for its ability to lower the interfacial
111 tension (IFT) between the NAPLs and water (γ_{ow}). Lauryl betaine (40%, LB, Cytec, CMC = 0.0125%)
112 was used to generate foam [18,19,24]. HCBD (97%, Alfa Aesar), which makes up to 58% of the
113 historical DNAPL was selected as a DNAPL model contaminant. For a better visualization of fluids
114 propagation in sandboxes, patent blue ($\geq 80\%$, VWR), tartrazine ($> 89\%$, Acros Organics) and eosin
115 ($\geq 85\%$, Acros Organics) were used as dyes to color the fluids. HCBD was dyed with oil red ($\geq 80\%$,
116 Sigma Aldrich). The tracers did not absorb onto the solid materials and had no significant influence
117 on formulations viscosity. Iron nanoparticles (NZVI) was procured as Nanofer 25 (Nanoiron). Table S1
118 summarizes the physical properties of NZVI, as gauged by the supplier. Acetone ($> 99\%$, Fisher) and n-
119 hexane (95%, Fisher) were used as solvents to extract the contaminants from soils. Other reagents
120 were potassium chloride (99.5%, Fisher), ammonium thiocyanate (99%, Sigma) and nitric acid (70%,
121 VWR). Compressed air was supplied by Air Liquide.

122 2.3. DNAPL characterization

123 The IFT between DNAPL and aqueous phase (γ_{ow}) was measured for pure water, SDBS 1.3×CMC (0.94
 124 g.l⁻¹) and LB 0.5% (40×CMC, 5 g.l⁻¹, used to make foam) using the pendant drop method [26,43]. The
 125 contact angle θ , at which the DNAPL-water interface meets a solid surface [44], was measured using
 126 the modified sessile drop method [45]. A glass microscope slide was used as a solid surface to mimic
 127 the glass beads soils used in this study. DNAPL density was measured using a pycnometer (25 ml ±
 128 0.04 ml) calibrated with ultrapure water, at room temperature. Viscosity measurements were carried
 129 out using the standard glass burette technique, according to Igathinathane [46].

130 2.3. DNAPL extraction in sandboxes

131 2.3.1. Experimental set-up

132 Two main methods were tested for DNAPL removal in sandboxes. First, NSTR was carried out where
 133 the propagation of fluids was dispersive since they were only controlled by injection forces. In
 134 addition to injection forces, the fluids propagation was also assisted by pumping with a vacuum
 135 system to induce their controlled converging flow. The STR was performed there, similar to
 136 multiphase extraction technology, the combination of fluid injection and pumping promotes NAPL-
 137 recovery by creating drawdown areas near the extractions wells [47]. The goal was to direct the
 138 fluids to the extraction well after the blocking of HPL. Experimental apparatus are presented in figure
 139 1.

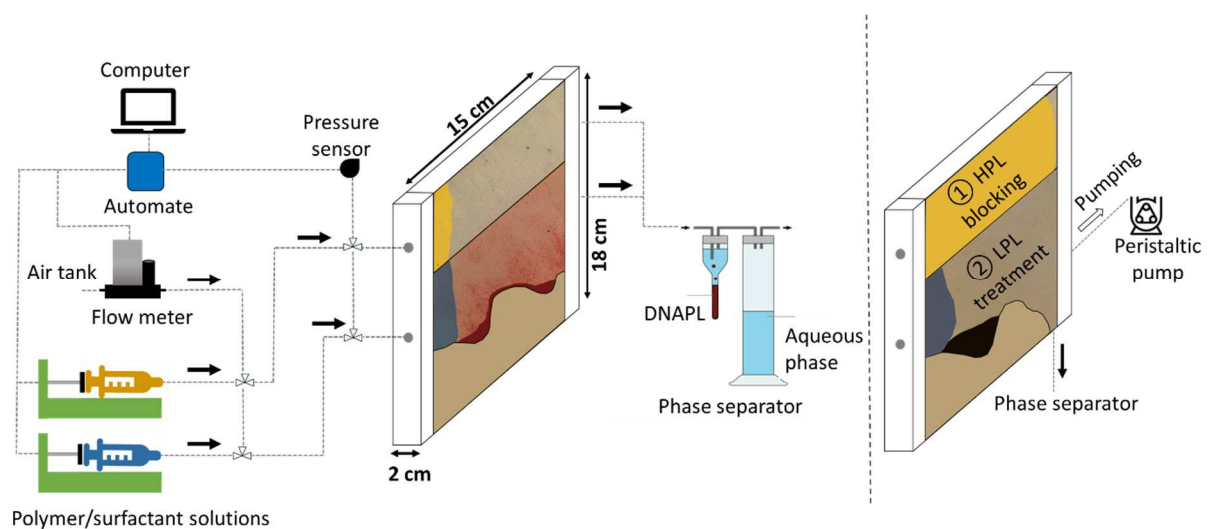


Figure 1. Trials equipment used for DNAPL extraction in sandboxes: non-spatially targeted DNAPL recovery (left) and spatially targeted DNAPL recovery (right).

140

141 The sandboxes (15 cm wide, 2 cm thick, 18.5 cm high, PMMA, porous volume (PV) = 121ml) were
 142 packed under water with the solid materials (HPL and LPL) and compacted using rubber stick while

143 filling. PV of HPL and LPL were 63 and 58 ml, respectively. The permeability contrast between the
 144 two porous materials was 10, as measured from the soil materials extracted from the contaminated
 145 site during non-destructive drilling operations. Regarding NSTR experiments, the water-saturated
 146 sandbox was contaminated with 7.7 ml of DNAPL (average saturation: 6.4%), which was injected
 147 from the top of the sandbox and placed as pools at the egg-box shaped clay/LPL (~95%) and at the
 148 LPL/HPL interfaces (~5%) using a syringe equipped with a needle while filling. The sandbox was
 149 equipped with two injection openings on the left side and two recovery points on the right side
 150 which were connected to a phase separator to quantify the amount of DNAPL recovered (Fig. 1 left).

151 To get closer to the real site configuration, where a welling system will be set up for DNAPL recovery,
 152 the clayey substratum was slightly modified for STR experiments, and a bottom DNAPL recovery
 153 point was connected to the phase separator [48]. During these experiments, 6 ml of the historical
 154 DNAPL (saturation: 4.8%) was placed as a pool in a single pit (Fig. 1 right). Good sealing of sandboxes
 155 was insured by placing a 10 mm-thick clay layer and a 5 mm-thick rubber plate, before covering the
 156 sandbox with a lid and clamping it. The front face of the sandbox was removable to allow for soil
 157 sampling at the end of the experiments.

158 For NSTR experiments, six fluids were injected from the left of the sandbox and compared to assess
 159 their ability to extract DNAPL, as summarized in table 1.

160 Table 1. Summary of the different DNAPL extraction experiments in sandboxes

	Fluid/experiment		[Xanthan] (g.l ⁻¹)	Surfactant	Contaminant
Non-spatially targeted recovery	Water		0	0	HCBD
	S		0	SDBS 1.3×CMC	
	X2		2	0	
	X2S		2	SDBS 1.3×CMC	
	Foam		0	LB 0.5%	
	X2SD		2	SDBS 1.3×CMC	
Spatially targeted recovery	- No HPL blocking	S	0	SDBS 1.3×CMC	Historical DNAPL
	- HPL blocking with foam	X01S	0.1	SDBS 1.3×CMC	
	- HPL blocking with xanthan	X02S	0.2	SDBS 1.3×CMC	

161

162 Each treatment step was carried out for all experiments, until the amount of DNAPL recovered
163 stopped increasing. First, pure water was injected as a reference fluid. Then, SDBS (S, $1.3 \times \text{CMC}$, 0.94
164 g.l^{-1}) was added to evaluate the effect of IFT lowering on DNAPL extraction. To evaluate the viscosity
165 effect alone on DNAPL removal, xanthan solution at 2 g.l^{-1} (X2) was used. The latter was then mixed
166 with SDBS at $1.3 \times \text{CMC}$ (X2S) to evaluate both the synergic effect of IFT-lowering and the viscosity on
167 DNAPL extraction. Surfactant foam (LB 0.5%, theoretical quality factor $F_{q,th} = 90\%$) was also tested as
168 mobilizing viscous fluid and compared to xanthan solutions [49]. Foamability and foam stability of LB
169 0.5% with and without HCBd were carried out according to [50]. Foamability with and without
170 DNAPL was 80 ± 5 and 85 ± 5 ml, respectively. Foam stability (time taken for the foam height to
171 decay to half the initial height) was 25 ± 3 and 525 ± 10 min with and without DNAPL, respectively.
172 For all the previous experiments, HCBd was used as a model of DNAPL. To get closer to field
173 conditions, an additional experiment was performed, consisting in the injection of a 2 g.l^{-1} xanthan
174 solution mixed with SDBS ($1.3 \times \text{CMC}$) in presence of the historical DNAPL (X2SD). The injected fluids
175 were colored in yellow and blue in HPL and LPL, respectively, for a better visualization of their
176 propagation. All the experiments were triplicated.

177 The remediation strategy was changed for STR experiments. First, the HPL was either blocked by
178 surfactant foam (LB 0.5%) or xanthan solution (2 g.l^{-1}) with surfactant ($1.3 \times \text{CMC}$), then fluids were
179 injected and pumped from the left to right of the LPL, respectively. A reference experiment without
180 blocking of the HPL (water circulation), was also carried out. Once the HPL was blocked, three fluids
181 were injected subsequently in the LPL until the amount of DNAPL recovered stopped increasing: first,
182 SDBS (S, $1.3 \times \text{CMC}$, blue), then xanthan solution at 0.1 g.l^{-1} mixed with SDBS $1.3 \times \text{CMC}$ (X01S, non-
183 colored), and finally, the xanthan concentration was doubled at 0.2 g.l^{-1} mixed with SDBS $1.3 \times \text{CMC}$
184 (X02S, blue). Moreover, after the HPL blocking, a red-colored water tank was connected to the HPL to
185 mimic the groundwater circulation and to evaluate the effectiveness of blocking. Table 1 summarizes
186 the experimental conditions used for STR. The rheological characterization of the studied non-
187 Newtonian fluids used in the experiments can be found in Section S1 in the supplementary materials.

188 2.3.2. Injection procedures

189 Solutions injection (pure water, SDBS, and xanthan solutions) was carried out for NSTR experiments
190 using a syringe pump (Pilot A2, Fresenius) and a dosing pump (KNF Simdos 10) connected to the LPL
191 and HPL, respectively. For all experiments, except the one with foam, fluids were injected
192 simultaneously in both layers at a flow rate of 4 ml.min^{-1} . For the experiment with foam, LB (0.5%)
193 and compressed air were co-injected into the sandbox using a syringe pump and a mass flow
194 controller (SLA5850, Brooks), respectively. Surfactant solution and gas flow rates were 8 and 70

195 ml.min⁻¹, respectively. The foam experiment was a two-step process: first, foam was injected in the
196 HPL to block it. Once the foam reached the edge of the HPL, foam injection was switched to the LPL
197 for DNAPL recovery.

198 For STR experiments, a peristaltic pump (Masterflex) was connected to the right of the sandbox at
199 the LPL outlet, creating a vacuum and a pumping process to increase the suction of the fluids to
200 induce their controlled flow. The flowrate of the peristaltic pump was constant and equal to the
201 injection flowrate in the LPL (4 ml.min⁻¹). Syringe pumps, flow meter, as well as solutions and gas
202 injection flow rates were the same as for NSTR experiments.

203 For all the experiments, the pressure at the injection point was monitored using a differential
204 pressure sensor (MPX5100DP, Freescale) and a limit of 1 bar.m⁻¹ was set to avoid conditions for soil
205 fracturing or upheaval [51].

206 2.3.3. Mass balance on DNAPL recovery

207 Mass balances calculations were performed from the NSTR extraction results obtained in sandboxes.
208 The experimental setup made it possible to measure the amount of contaminants still present in all
209 the treated soil since the front face of the sandbox was removable. Besides, the contaminant
210 recovered in the phase separator either as pure phase or dissolved in the water phase was evaluated.
211 The contaminant in the aqueous phase remaining in the sandbox was also considered. Mass balance
212 calculations were performed from the initial mass of DNAPL introduced into each experiment.

213 2.4. Iron nanoparticles injection

214 For further removal of the COHs left after DNAPL-recovery, NZVI injection was tested. NZVI proved to
215 be effective in degrading a broad range of organic pollutants in groundwater systems, especially
216 COHs [37–40,52]. Since NZVI in pure water is not stable due to fast aggregation and sedimentation
217 [53,54], NZVI suspensions (1 g.l⁻¹) were prepared in a 2.2 g.l⁻¹ xanthan solutions. The slightly higher
218 xanthan concentration was selected to compensate the solution viscosity decrease. Indeed, the
219 addition of iron nanoparticles causes the perturbation of the associative behavior of xanthan,
220 resulting in a decrease in viscosity [27]. Suspensions were dispersed using a high-performance
221 dispersing device at 25000 rpm for 5 min. (ultra-turrax®, IKA T25) before injection. This study only
222 focuses on the injectability and behavior of the suspensions.

223 2.4.1. Breakthrough curves in columns

224 Before the injection of NZVI in sandboxes, breakthrough curves in HPL and LPL packed glass columns
225 (l: 0.4 m, i.d.: 3.2 cm) were carried out to assess their transport in these porous media. The freshly

226 prepared NZVI suspensions were injected at a flow rate of 8 ml.min⁻¹. Fractions of 10 to 20 ml
227 leachates were collected from the column outlet in 50 ml glass flasks. A total of 4 PV were injected.
228 The collected leachates were then analyzed to determine NZVI concentrations. A non-reactive tracer
229 (KCl, 1 g.l⁻¹) was also injected for control and baseline measurements and the conductivity of the
230 effluent was also monitored (Consort C8862).

231 Breakthrough curves were obtained by plotting the ratio of the NZVI concentration C measured in
232 the effluent at time t and the one in the injected fluid C_0 , vs. time. It is possible to estimate of the
233 Darcy velocity u (m.s⁻¹) and the dispersivity of tracers α (m) by using the advection-dispersion
234 equation solution in semi-infinite column [55]:

$$235 \frac{C}{C_0} = 0.5 \cdot \left[\operatorname{erfc} \left(\frac{x-u.t}{\sqrt{4.\alpha.u.t}} \right) + \exp \left(\frac{x.u}{D} \right) \cdot \operatorname{erfc} \left(\frac{x+u.t}{\sqrt{4.\alpha.u.t}} \right) \right] \quad (1)$$

236 where x (m) is the length of the column and D (m².s⁻¹) is the dispersion coefficient.

237 When x/α is large, the second term can be neglected and the eq. 1 becomes:

$$238 \frac{C}{C_0} \sim 0.5 \cdot \operatorname{erfc} \left(\frac{x-u.t}{\sqrt{4.\alpha.u.t}} \right) \quad (1')$$

239 Values of u and α were fitted from the breakthrough curves of KCl for HPL and LPL, assuming it is a
240 conservative tracer. Setting the obtained α -value, the retardation factor for the NZVI in xanthan
241 solution was then calculated for both media, as the ratio of the Darcy velocities fitted from the KCl
242 and the NZVI breakthrough curves, respectively. Besides, considering some irreversible trappings of
243 NZVI, a transmission factor was calculated from the plateaus-value of the C/C_0 ratio at long times,
244 assuming a permanent regime was established.

245 At the end of the transport experiments, the columns were sacrificed to measure the spatial
246 distribution of NZVI. The columns were dissected into 20 segments 2 cm-thick and the average NZVI
247 concentration was measured in each section to better assess NZVI retention.

248 2.4.2. Injection of NZVI in sandboxes after DNAPL recovery

249 Two strategies were tested in sandboxes for the NZVI (1 g.l⁻¹) injection. Using the first one, NZVI in
250 xanthan (2 g.l⁻¹) was injected into the LPL at 5 ml.min⁻¹ after the X2SD treatment. During this
251 treatment, the injection of xanthan solution was maintained in the HPL while injecting the NZVI in
252 the LPL. The second one was a three-step process: first, the HPL was blocked by the co-injection of
253 gas and a xanthan solution (1 g.l⁻¹) with SDBS (1.3×CMC) to create viscous foam (blue). Second, X2SD

254 (yellow) was injected into the LPL for the DNAPL recovery. Finally, once DNAPL recovery was
255 achieved, NZVI in xanthan solution was injected into the LPL at 5 ml.min⁻¹.

256 2.5. Analytical methods

257 2.5.1. DNAPL determination in media

258 For NSTR experiments with HCBd, the latter was extracted using a Soxhlet from the LPL after
259 homogenization. The solids were extensively washed by recycling 80 ml of a hexane/acetone mixture
260 (1/1w), for 4h, in a heated reflux (110°C). The recovered organic phase was reported to 100 ml and
261 diluted if necessary. It was then dehydrated with anhydrous sodium sulphate before analysis. HCBd
262 analysis in water effluents was carried out directly in headspace. Both analyses were carried out by
263 GC-MS (Perkin Elmer and ThermoFisher for soils and water, respectively), according to the NF EN ISO
264 10301-3 standard.

265 For the X2SD experiment with the historical DNAPL, the semi-volatile C10-C40 fraction in the soil and
266 water effluents was analyzed by GC-FID according to the NF EN ISO 9377-2 standard after the
267 homogenized soil from LPL or 10 ml of water was extracted with n-hexane. For the volatile C5-C11
268 fraction, the soil was washed with acetone and the recovered organic phase was then analyzed by GC
269 according to the XP T90-124 standard. For water effluents in XS2D experiment, the C5-C11 fraction
270 was analyzed directly in headspace using GC-MS.

271 2.5.2. Iron determination

272 For column leachates, 30 to 100 µl were transferred in glass flasks with 2 ml deionized water and 1
273 ml nitric acid (10 mol.l⁻¹). Then, 2 ml NH₄SCN (2 mol.l⁻¹) were added to filtrates to form the Fe(SCN)²⁺
274 complex. For solid samples, 2 g of sampled soil across the column were transferred in a glass flask
275 with 10 ml deionized water and 4 ml nitric acid. Then, the flask was shaken using an orbital shaker for
276 30 min to extract iron into the water phase. Then, the samples were filtered through a syringe filter
277 (0.45 µm), diluted if necessary and 2 ml NH₄SCN (2 mol.l⁻¹) was added. Finally, the Fe(SCN)²⁺ complex
278 was quantified by UV-vis spectrometry (Agilent Cary 100) at 478 nm [56].

279 3. Theory

280 For sandbox treatment steps, capillary, bond, and total trapping numbers (N_{ca} , N_B and N_T
281 respectively) were calculated. Considering the balance between capillary, viscous and gravity forces
282 on trapped DNAPL droplets at the pore scale, their onset displacement is associated to the total
283 trapping number N_T [57]:

284
$$N_T = \sqrt{N_{ca}^2 + 2 \cdot N_{ca} \cdot N_B \cdot \sin \alpha + N_B^2} \quad (2)$$

285 where α is the angle is the angle of flow relative to the horizontal, while N_{ca} is the capillary number
 286 of the injected fluid and N_B is the Bond number defined as follows:

287 - N_{ca} is a dimensionless quantity that amount the ratio of viscous to capillary forces:

288
$$N_{ca} = \frac{u_w \cdot \eta_w}{\gamma_{ow} \cos \theta} \quad (3)$$

289 where u_w and η_w are the Darcy velocity and the dynamic viscosity of the injected fluid, respectively.

290 - N_B represents the ratio of the buoyancy to capillary forces

291
$$N_B = \frac{g \cdot k \cdot k_{rw} \cdot \Delta\rho_{ow}}{\gamma_{ow} \cos \theta} \quad (4)$$

292 where k and k_{rw} are the soil permeability and the local relative permeability of water, g is the
 293 gravitational acceleration and $\Delta\rho_{ow}$ is the density difference between the non-miscible fluids.

294 Based on transport equations in coupled systems, the following relationship between the DNAPL
 295 residual saturation and N_{ca} has been proposed [58]:

296
$$S_{or} = S_{or}^{min} + (S_{or}^{max} - S_{or}^{min}) [1 + (T_1 N_{ca})^{T_2}]^{\frac{1}{T_2} - 1} \quad (5)$$

297 where S_{or} is the residual NAPL saturation, S_{or}^{max} and S_{or}^{min} are the residual saturations before and
 298 after mobilization, respectively. T_1 and T_2 are fitting parameters, which control the onset of
 299 mobilization and the fall of the desaturation curve, respectively.

300 4. Results

301 4.1. DNAPLs characterization

302 The physicochemical properties of HCBd and the historical DNAPL with the different fluids used in
 303 this study are summarized in table 2.

304 Table 2. HCBd and historical DNAPL physicochemical properties in different conditions used in this
 305 study.

	Water		SDBS (1.3×CMC)		Xanthan (2 g.l ⁻¹)		LB 0.5%		η	d
	γ	θ	γ	θ	γ	θ	γ	θ		
HCBd	38±7	127±7	2.0±0.6	63±4	38±7	136±6	2.0±0.9	0	2.44	1.66
DNAPL	31.5±2.0	122±5	0.68±0.08	54±3	31.5±2.0	128±4	1.1±0.2	0	4.47	1.68

306 γ : Interfacial tension ($\text{mN}\cdot\text{m}^{-1}$) at the DNAPL/water interface; θ : Contact angle ($^\circ$) between
307 glass/DNAPL/water; η : dynamic viscosity ($\text{mPa}\cdot\text{s}$); d : density

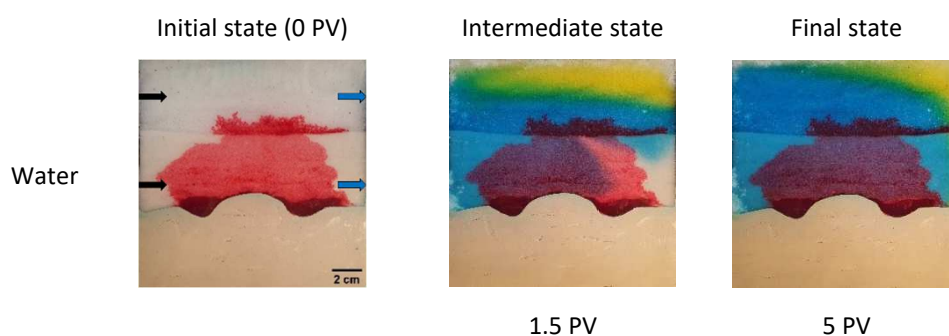
308

309 As seen from table 2, HCBd and the historical DNAPL had similar densities of 1.66 and 1.68,
310 respectively, which can be explained by the fact that major COHs components have density ranging
311 from 1.6 to 1.8. Yet, the historical DNAPL was 1.8-times more viscous which could be linked to its
312 complex composition and age. In fact, as DNAPLs lose the lighter components from dissolution, they
313 become more viscous as the heavier components compose a larger fraction of the oily mixture
314 resulting in an increase in viscosity [59]. The DNAPLs had similar IFTs and contact angles in presence
315 and absence of xanthan in aqueous solution, showing that the presence of the polymer had
316 negligible effect. IFT values were high and similar to those previously reported for chlorinated
317 compounds/water systems [60]. In absence of surfactant, $\theta > 90^\circ$ for HCBd and historical DNAPL
318 resulted from their hydrophobicity, suggesting that the DNAPLs were the non-wetting fluids in
319 absence of surfactants [59]. As expected, the addition of surfactant (SDBS $1.3\times\text{CMC}$ or LB 0.5%
320 ($40\times\text{CMC}$)) led to the significant decrease of IFTs and θ for both DNAPLs [61–64]. The presence of
321 xanthan had no effect on both IFTs and θ in presence of surfactant. However, it is noteworthy that
322 IFT lowering was more efficient in presence of historical DNAPL (2.4-times lower in average). Contact
323 angles were also lower when adding surfactant for historical DNAPL (63 ± 4 vs. 54 ± 3). Contact angles
324 were zero (flat droplets) for both DNAPLs when using LB 0.5% is explained by the presence of a more
325 concentrated surfactant solution ($40\times\text{CMC}$) needed to make strong foams quickly.

326 4.2 NSTR experiments

327 4.2.1 Comparison of DNAPL extraction fluids

328 The visual comparison of the six extracting fluids for NSTR experiments is shown in figure 2.



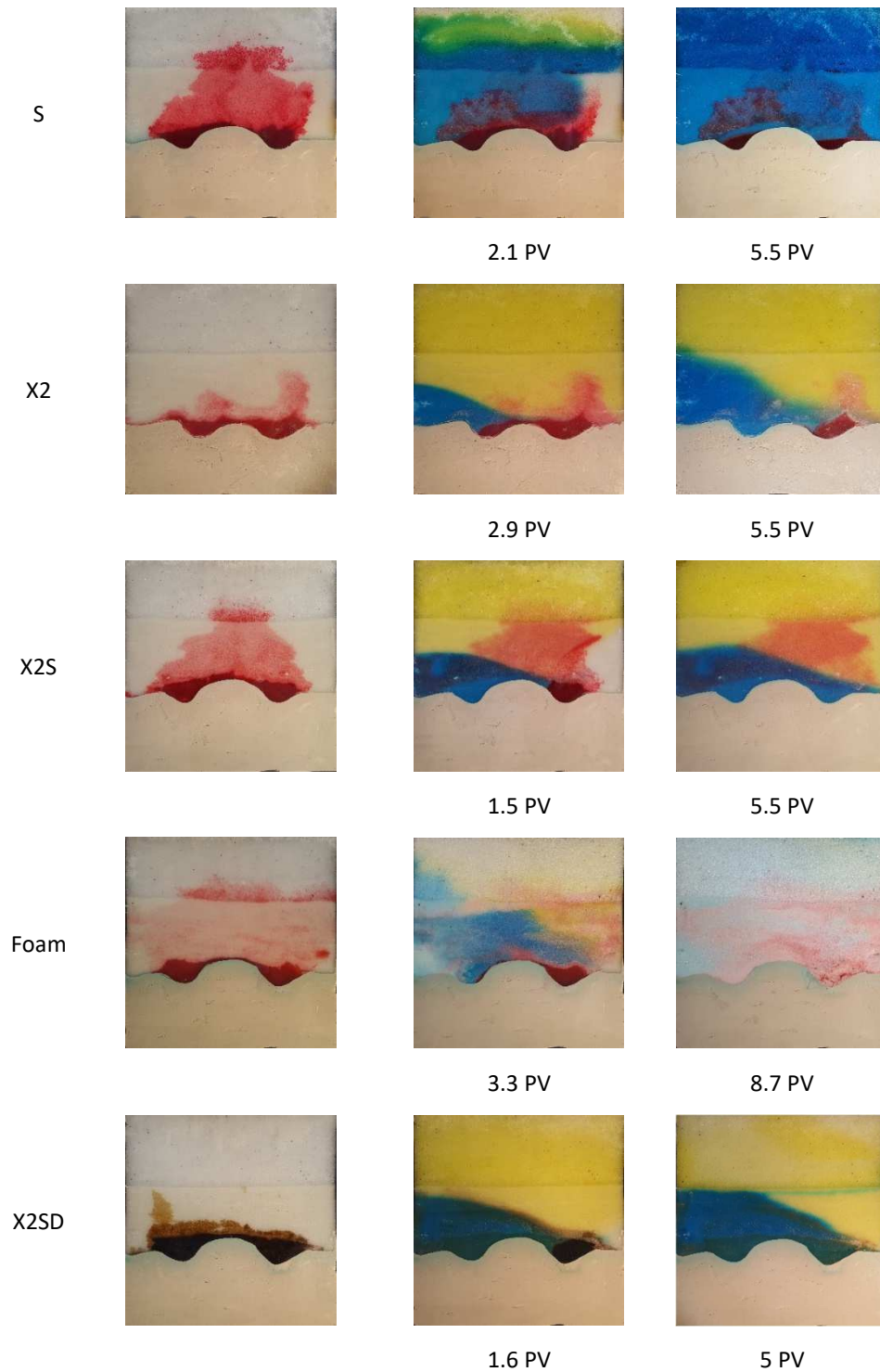


Figure 2. Comparison of DNAPL recovery in sandboxes using different flushing fluids for NSTR experiments. Flow direction is from the left to the right. Injected fluids were blue and yellow for LPL and HPL, respectively. Except for X2SD experiment (black color of the historical DNAPL used), the model DNAPL (HCBD) was colored in red. Black and blue arrows show injection and recovery points, respectively.

329 When water and S were injected in the LPL, both liquids flowed preferentially in the more permeable
 330 HPL layer, given the latter's lower hydraulic resistivity. Mixing between the two solutions was also
 331 observed from the appearance of a green color in the HPL. Table S3 summarizes capillary, bond and
 332 total trapping numbers for NSTR and STR experiments. Despite an improved N_{ca} -value, S was not able
 333 to mobilize DNAPL from the pits in the substratum. Velocity contrasts were 2.5 and 2.2-times faster
 334 between the HPL and the LPL for water and S, respectively. This shows that the local permeability
 335 contrast was lowered for the superposed materials in sandbox.

336

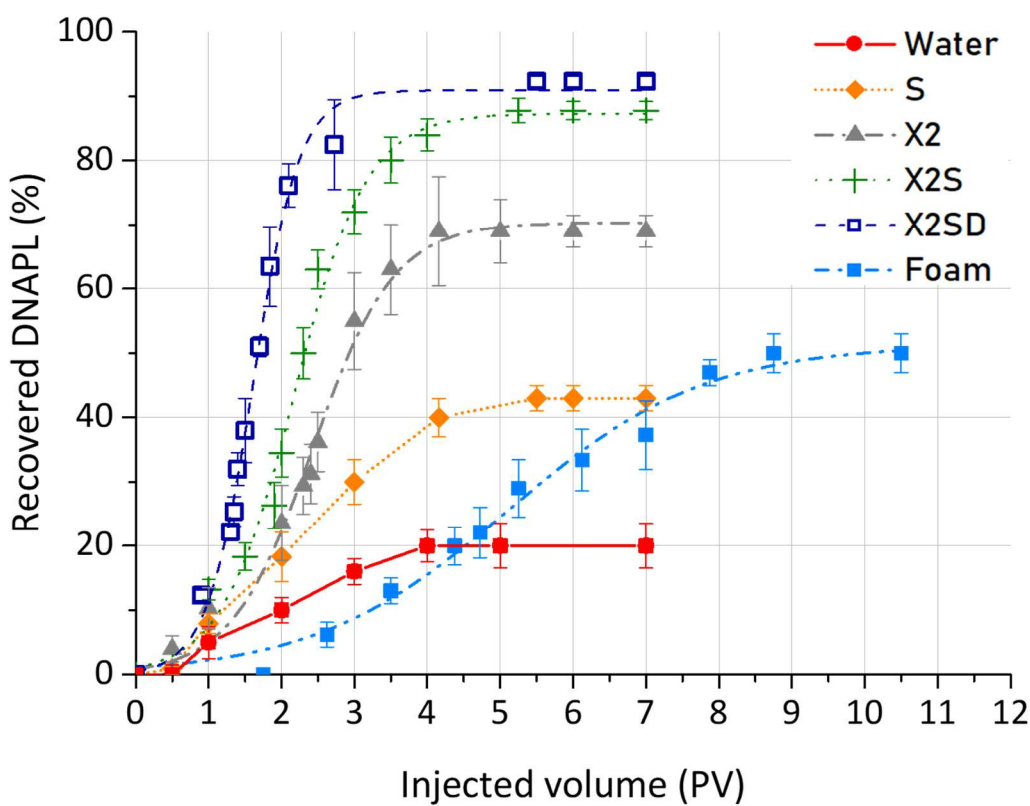


Figure 3. Comparison of DNAPL recovery vs. injected PV for the different flushing fluids in non-spatially targeted DNAPL recovery (NSTR) experiments in sandbox.

337

338 For X2, X2S and X2SD experiments, and conversely S water. Here, the rheology of xanthan solutions
 339 in bulk and in both soils was similar, demonstrating that the shear-thinning behavior increases with
 340 the shear-rate in these soils. A crossflow behavior was observed from the HPL to the LPL as
 341 previously observed [65,66]. It resulted in a beveled shape xanthan front between the two zones,
 342 caused by different velocities. The crossflows forced the injected solution in the LPL, enhancing the

343 sweeping at the bottom of the substratum where most of the contaminant stood. The addition of
344 SDBS $1.3 \times \text{CMC}$ in the xanthan solution led to a slight decrease in viscosity resulting from the
345 perturbation of the associative behavior of xanthan (see Fig. S2). Nevertheless, X2S viscosity remains
346 3 orders of magnitude higher than that of pure water. The injectability of the three solutions was
347 good (see figure S3). Propagation velocities were about 0.5 m.d^{-1} for xanthan solutions which is
348 approximately 6-times slower than pure water injection velocity. In the presence of xanthan, an
349 efficient displacement of the contaminant linked to a continuous DNAPL phase was observed at the
350 top of the substratum which led into the outlet. Here, DNAPL displacement occurred in two regimes:
351 first, the increase in N_{ca} and the formation of a DNAPL bank. Then, the N_{ca} remained nearly constant,
352 and the DNAPL was moved droplet by droplet as a dispersed phase [67]. Downstream of the DNAPL
353 bank, some contaminant was mobilized as a microemulsion. Nevertheless, for X2 the second pit of
354 DNAPL was not efficiently swept, probably due to an insufficient N_{ca} -value compared to X2S and
355 X2SD (see table S3). After 5 PV on average, contaminant recovery was 70, 87 and 93% for X2, X2S and
356 X2SD, respectively. The recovery differences between experiments can be explained by the lower
357 IFTs and θ in presence of surfactant (table 2).

358 Figure 3 compares the DNAPL recovery as a function of injected PV for the different flushing fluids. A
359 different behavior than water and S was obtained in presence of xanthan. Here, an “S-shape”
360 recovery was noted, which shows an increase in the efficiency of DNAPL removal. The latter started
361 immediately without lag volume, then accelerated in a second phase before decreasing when
362 approaching the plateau. The similar observed behavior was due to the viscous effect of the injected
363 fluid and the capillary pressure exerted on the DNAPL. The fast DNAPL recovery taking place as soon
364 as the polymer enters the sandbox, suggests that these forces allowed the DNAPL to penetrate the
365 pores and reconnect to the outlet. This led to an efficient displacement of the DNAPL upstream of
366 the flat front. The recovery accelerates between 1.5 (X2SD) and 2 PV (X2, X2SD) depending on IFT-
367 values. For X2SD, where the lowest IFT was obtained, the most effective piston-like displacement of
368 the DNAPL was observed—and 93% of the initial contaminant was removed. Residual contaminant
369 saturations were calculated to be 1.6, 0.66 and 0.22% for X2, X2S and X2SD, respectively. Through
370 the plateau values, it was noticeable that the IFT effects allowed to gain up to 27% additional
371 recovery (X2 vs. X2S), while the viscosity allowed to gain approximately an additional 45% (S vs. X2S).

372 Surfactant foam was also compared to polymer solutions since it also exhibited a shear-thinning
373 behavior widely investigated for DNAPL recovery [25,26,49,68]. Here, foam was subsequently
374 produced in both layers propagated as a flat front, while crossflow was observed between the two
375 zones [18,69,70]. Contrasts between fluid velocity were 36% lower compared to pure water thanks

376 to the shear-thinning behavior of foam. Foam injectability was quite bad since its velocity was 17-
 377 times lower than the imposed one. Foam managed to sweep the first pit of the substratum but not
 378 completely the second one due to insufficient viscosity and density effects in the LPL compared to
 379 xanthan solution (see table S3). The HCBD recovery curve shown in figure 3 was linear and exhibited
 380 a lag volume of 1.9 PV similarly to water and S. The particular delay associated with the foam is
 381 probably due to the transient regime at the beginning of the injection which results in weak foam.
 382 Expressed in PV of the injected liquid, the slope associated with the DNAPL recovery by the foam is
 383 greater than for S and water. The plateau was reached at a 50% recovery, indicating that the viscous
 384 effects were weak. Besides, a fraction of gas bubbles tended to rest at pore throats and blocked
 385 them where trapped ganglia of HCBD were still present. This reduces the connectivity between the
 386 pores of the soil. Furthermore, it led to the bypass of some contaminated pore throats that were
 387 blocked, to the creation of dead ends, and to the redirection of flow elsewhere. Additionally, HCBD
 388 may have had a destabilizing effect on foam formation (see §2.3.1) as previously observed [71,72].

389 Even though the trapping of DNAPL and the used reagents may be more important in some real soils
 390 than the model ones used here, it is still relevant to compare the remediation fluids regarding the
 391 variety of natural soils and reagents. As previously reported, while it takes up to a few months for a
 392 typical xanthan solution to be leached by large volumes of groundwater, surfactant is removed from
 393 injected foam very quickly [8,73]. Figure 4 displays the capillary desaturation curve obtained from the
 394 different NSTR experiments. It relates residual DNAPL saturation to the N_{ca} -value of each treatment.
 395 Through the different treatment processes involved, all the points can be joined and fitted using Eq.
 396 5 ($r^2 > 0.99$).

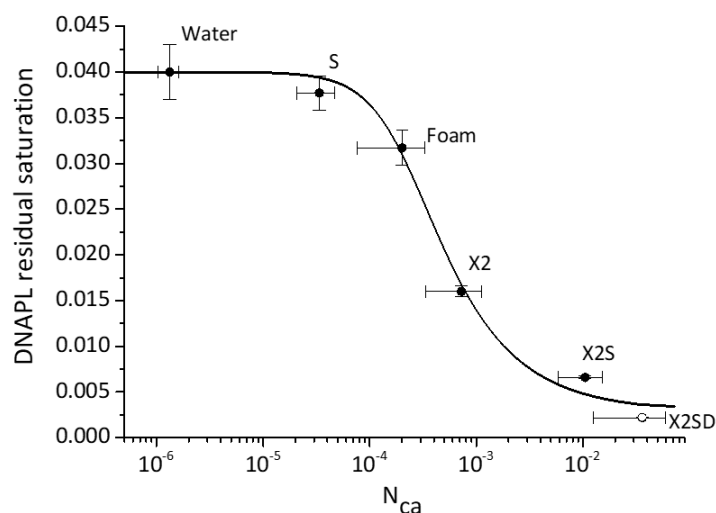


Figure 4. DNAPL residual saturation vs. N_{ca} for NSTR using different flushing fluids. Solid black dots: HCBD. Open dot: historical DNAPL.

397

398 For injected fluids with N_{ca} -values lower than 10^{-5} , the residual saturation of DNAPL remained
399 essentially constant as the flushing fluids were unable to overcome trapping forces that retained
400 DNAPL droplets. Similar observations were reported for Ottawa sand columns surfactant flushing
401 contaminated with PCE, TCE and jet fuel [57,74] and for polymer flushing of limestones contaminated
402 with PCE [75]. Then, when the N_{ca} was increased beyond 10^{-5} , the residual saturation of DNAPL
403 decreased below 0.006, which enables polishing treatment like chemical degradation at reasonable
404 cost.

405 Fitting parameters of Eq.5 (T1 and T2, see table S4) were very similar to the data from Maire [25] as a
406 result of close experimental conditions. In fact, T1 controlled the onset of DNAPL mobilization; as T1
407 was decreasing, mobilization occurred at higher N_{ca} and N_T [58]. T2 controlled the desaturation curve
408 shape; a higher T2 was associated with a steeper desaturation curve. In fact, T2 increased with the
409 soil permeability which led to an easier desaturation when the capillary suction was lower.

410 4.2.2. Mass balances on COHs

411 Results of mass balances on COHs (recovered as pure phases, dissolved in water effluents, and
412 remaining in the solid material) after NSTR treatments are summarized in table 3 (see table S5 for
413 more details).

414 Table 3. Mass balances results after NSTR mobilization experiments using different flushing fluids.

Experiment	Pure phase DNAPL recovery (%)	Dissolved DNAPL in effluents (%)	Dissolved DNAPL in effluents (mg.l^{-1})	Total DNAPL recovery (%)	Remaining DNAPL in soil after treatment (%)	$[\text{DNAPL}]_{\text{treated LPL}}$ (mg.kg^{-1})	Total recovery (%)
Water	20.83	0.00046	0.18	20.83	76.62	11281	97.45
S	42.98	0.008	1.5	42.98	45.65	8536	88.63
X2	68.97	0.0012	0.32	68.96	24.30	5000	93.26
X2S	87.80	0.0197	5.4	87.82	9.60	2040	97.42
X2SD	92.55	0.1570	33	92.70	3.92	768	96.62
Foam	49.93	0.02	53	49.95	46.31	9800	96.26

415

416 High total recovery rates on mass balances were obtained for all the experiments, characterized by a
 417 median value of 96.4%. Low surfactant concentrations near CMC-values led to low DNAPLs
 418 solubilization in the water effluents. Despite low SDBS concentrations ($1.3 \times \text{CMC}$), a net increase, by
 419 an order of magnitude, of COHs concentrations in water effluents was observed. This is believed to
 420 result from some DNAPL emulsification rather than from micellar solubilization. The highest COH-
 421 concentration in effluents (53 mg.l^{-1}) were obtained with foam experiment, in which a high surfactant
 422 concentration ($40 \times \text{CMC}$) was used. Mass balance calculations revealed that the lowest COH-
 423 concentration in soil after flushing was obtained for X2SD. In this case, the historical DNAPL
 424 concentration in LPL was 768 mg.kg^{-1} , which is still high considering remedial goals. A polishing
 425 treatment is required to further decrease this concentration. For this reason, NZVI injection
 426 experiments were carried out in column and sandbox (see §4.4).

427 4.3. Spatially targeted DNAPL recovery

428 The visual comparison of the three strategies tested for the spatially targeted DNAPL recovery
 429 experiments are shown in figure 5.

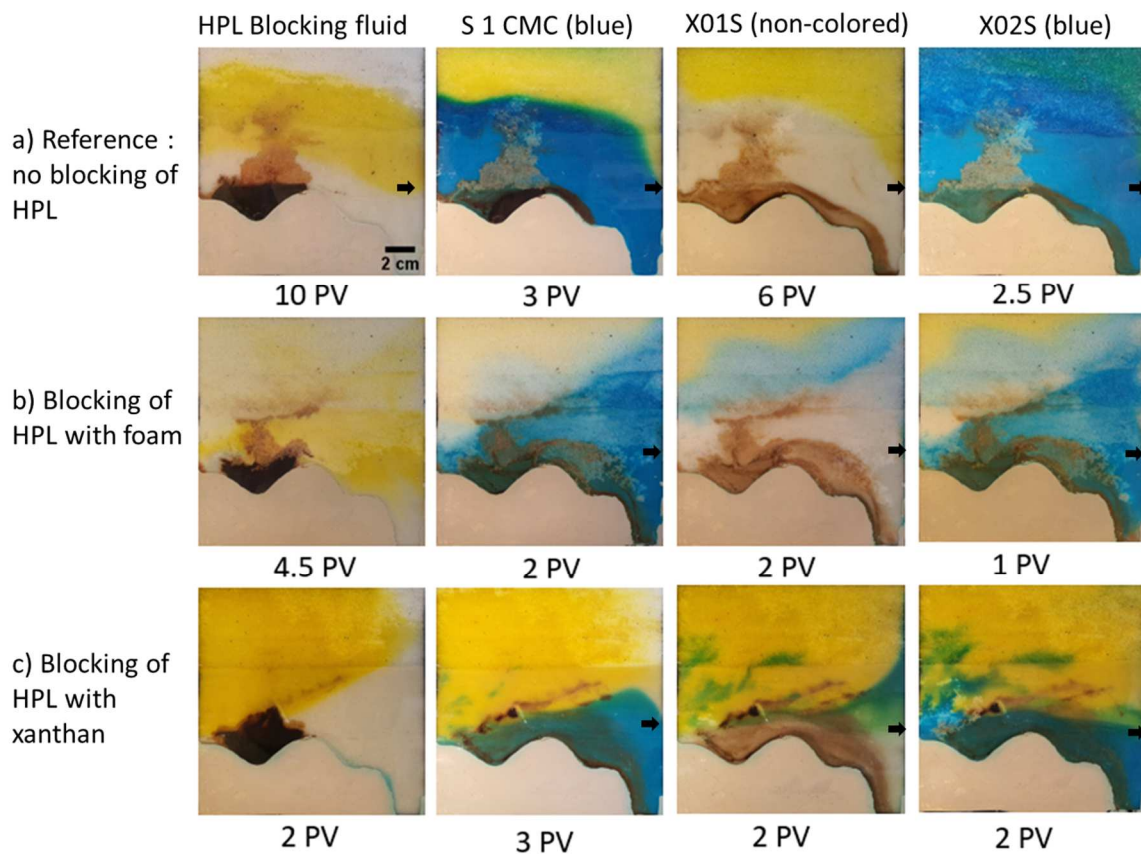


Figure 5. Comparison of DNAPL recovery in sandboxes using different flushing fluids for STR experiments. The flow direction is from left to right. Fluids injected in the HPL were water (top

line), surfactant foam (middle line) and xanthan solution (bottom line). Flushing fluids (S, X01S and X02S) were injected in the LPL after blocking of the HPL. The black arrows show the position of the pumping system. PV indicates the injected pore volume at each step.

430
 431 When groundwater circulation in the HPL was not blocked (Fig. 5 top), the latter was controlled by
 432 the vacuum system, which explains the yellow-colored tilted pathway. Conversely, surfactant foam
 433 and a solution xanthan (2 g.l^{-1}) with surfactant ($1.3 \times \text{CMC}$) were injected in the HPL to block it and
 434 minimize preferential paths. Both fluids migrated in the HPL with a crossflow in the LPL due to their
 435 shear-thinning behavior. For both cases, the HPL was blocked well enough, since no red color
 436 simulating groundwater flow was observed when the pumping system was set-up.
 437 Then, surfactant ($1.3 \times \text{CMC}$, blue) was injected and pumped from the left to right of the LPL, while
 438 the circulation in the HPL was maintained. Figure 6 summarizes the DNAPL recovery after each step
 439 for STR experiments.

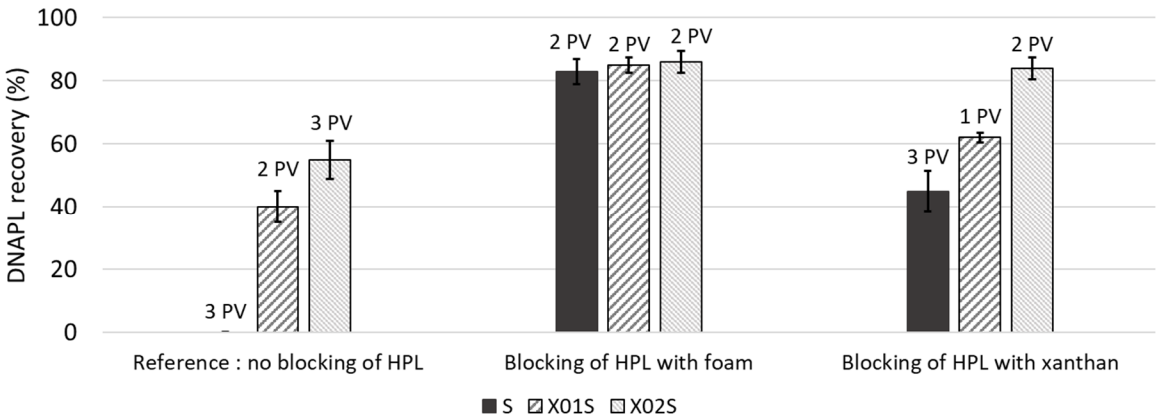


Figure 6. DNAPL recovery for STR experiments with SDBS $1.3 \times \text{CMC}$ (S), xanthan 0.1 g.l^{-1} + SDBS $1.3 \times \text{CMC}$ (X01S) and xanthan 0.2 g.l^{-1} + SDBS $1.3 \times \text{CMC}$ (X02S).

440
 441 During this step, no DNAPL was recovered when the HPL was not blocked due to insufficient viscous
 442 forces. DNAPL recovery reached 83 and 45% after 2 and 3 PV for foam and xanthan blocking
 443 experiments, respectively. When the HPL was blocked by foam, the DNAPL-recovery was 2-times
 444 higher than for the S experiment in NSTR with the same N_{ca} (see fig.3). This showed a strong
 445 improvement in the LPL-sweeping and an increase in the pressure during S propagation in the LPL
 446 compared with no blocking of HPL as shown in Figure S4, summarizing the pressure profiles for ADR
 447 experiments. Fingering was observed for the xanthan blocking since surfactant solution was probably
 448 injected too close to the viscous xanthan one, which can explain those differences and the lower

449 pressure recorded for S in this case (see Fig. S4). Additionally, a fraction of the DNAPL (~11%) was not
450 recovered because trapped in the outer limit of the yellow blocking xanthan solution.

451 Then, the surfactant solution was replaced with colorless X01S and blue X02S, which were injected
452 and pumped simultaneously. The final DNAPL recoveries ranged from 55 to 86% in absence and in
453 presence of HPL-blocking, respectively. The high DNAPL recoveries for foam and xanthan blocking
454 experiments were similar to those obtained during NSTR experiments, however the polymer was 10
455 to 20-times less concentrated. Indeed, It was previously reported that applying a vacuum increased
456 the effective drawdown locally near the pumped well [76]. Moreover, the induced vacuum increased
457 the liquids flow rates and the DNAPL extraction rates due to the increased pressure gradient applied
458 to the system. Indeed, Darcy flow rates were enhanced by one order of magnitude on average
459 between NSTR and STR experiments. In fact, thanks to the vacuum system, which made converging
460 flows, fluids with a 3-times lower N_{ca} (see table S3) and a 10 to 20-times lower concentration in
461 xanthan allowed similar recoveries than for the X2S experiment (see Fig.3).

462 No matter whether the HPL was blocked with some foam or some xanthan solution, the induced flow
463 allowed to reach some high DNAPL recovery rates with fewer viscous and non-dense fluids than
464 NSTR. It was also slightly more efficient when using foams. Modeling can be a valuable tool for
465 blocking with xanthan solution to position the apertures of injection and recovery wells regarding the
466 depth of geological layers. Also, this technique is especially suitable for contaminant removal from
467 fine grained formations (hydraulic conductivity from 10^{-5} to 10^{-7} m.s⁻¹) [47,76]. Lastly, would create
468 larger radii of influence which would require significantly fewer wells due to its ability to maximize
469 fluid recovery at the wellhead [47,76].

470 4.4. Iron nanoparticles injection

471 As seen from sandbox experiments, residual DNAPL was still present after flushing and the lowest
472 residual DNAPL concentration was 768 mg.kg⁻¹ (XS2D treatment, see table 3). Further treatment is
473 needed to achieve satisfactory remedial goals. For this reason, NZVI injection was tested in columns
474 and sandboxes.

475 4.4.1. Column studies

476 NZVI were delivered in xanthan solutions because of the enhanced suspension stability and hindered
477 particles aggregation [77–79]. In this study, the injected NZVI concentration was 1 g.l⁻¹ given the
478 theoretical concentration required to completely degrade the residual DNAPL.

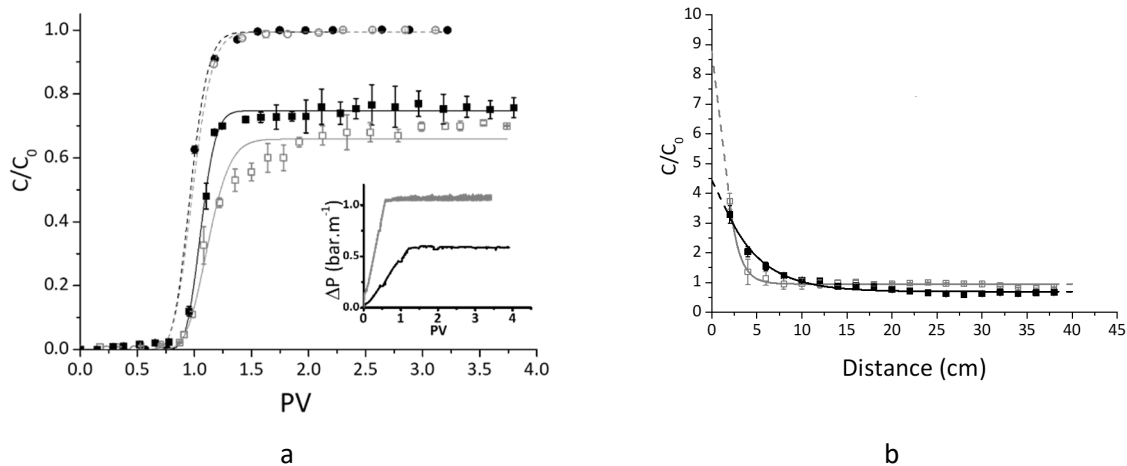


Figure 7. a) Breakthrough curves of NZVI (1 g.l^{-1} , solid lines) in xanthan solution in: a) LPL (\square) and b) HPL (\blacksquare) and KCl (conservative tracer, 1 g.l^{-1} , dashed lines) in c) LPL (\circ) and d) HPL (\bullet). Insert: Pressure gradients for NZVI injection in LPL (grey) and HPL (black). b) NZVI concentration variations along the soil columns after the experiments for HPL (black) and LPL (grey).

479

480 Breakthrough curves in the HPL and the LPL materials for KCl and NZVI delivered in xanthan solutions
 481 are shown in figure 7a. The plateaus for the transmission of NZVI through the columns reached
 482 maximums of 0.73 and 0.65 at 1.5 and 2 PV for the HPL and the LPL materials, respectively. The
 483 plateau was reached more rapidly for KCl, which travelled like a conservative tracer. Similar
 484 observations were reported for the transport of CMC-NZVI at 1 g.l^{-1} in fine and in coarse sand
 485 columns [80]. The higher C/C_0 value for HPL, and thus the higher NZVI mobility were explained by
 486 bigger pore sizes of media made of coarser grains. At permanent regimes, bigger NZVI retention (27%
 487 for HPL vs. 35% for LPL) through the LPL stemmed from lower pore sizes which led to stronger sieving
 488 but also sorption due to higher surface area of the soil material [81]. Nevertheless, both soils were
 489 not completely blocked after 4 PV, which suggested that the attachment capacity of the soils was
 490 not exhausted. This was especially true for HPL, since the pressure gradient at the plateau (0.6 bar.m^{-1}
 491 $^{-1}$) was lower than the fixed limit of 1 bar.m^{-1} during the injection process (see insert Fig. 7a). The
 492 average Darcy velocities for NZVI injection were obtained from eq.1' fitting after fixing dispersivity
 493 values of 3.3×10^{-3} and $3.7 \times 10^{-3} \text{ m.s}^{-1}$ obtained from fitted KCl curves through the HPL and the LPL
 494 materials, respectively. Retardation factors of 1.08 and 1.14 were calculated for NZVI transmission
 495 for HPL and LPL, respectively. This demonstrated good injectability and transmission of the NZVI
 496 suspensions through both soils.

497 After the NZVI transport experiments, the soil columns were sacrificed and the iron concentration was
 498 measured in each 2 cm-ports from the input (Fig. 7b). NZVI accumulation was observed at the

499 column input for both soils which explained C/C_0 values larger than 1. It decreased exponentially with
500 the distance as clogging decreased to reach 0.67 and 0.85 for the HPL and the LPL materials which
501 represents a respective decrease of 79% and 77%. The reduction of NZVI concentration along the
502 increase in distance from the injection point was reported by many [22,54,77,82,83]. Given the
503 balance equation on amendment injection through a filter medium, this exponential behavior is
504 explained by a concentration gradient along the distance (d) which is proportional to the
505 concentration [8]. Experimental data were fitted using the following eq. :

$$506 \frac{C}{C_0} = T + \Delta T \cdot e^{(-k \cdot d)} \quad (6)$$

507 Where T is the NZVI transmission-accumulation factor, ΔT is the amplitude of the NZVI accumulation,
508 and k (cm^{-1}) is filtering constant relative to the soil.

509 T -values of 0.70 ± 0.03 and 0.95 ± 0.01 and k -values of 0.25 ± 0.02 and $0.92 \pm 0.07 \text{ cm}^{-1}$ were
510 obtained for the HPL and the LPL materials, respectively. Larger T , and k -values obtained for LPL
511 confirm that NZVI was more retained by the finer soil. Similar trends and values for fitting
512 parameters were reported for similar experimental conditions [19, 75].

513 4.4.2. Sandbox studies

514 Two main strategies were tested for the delivery of NZVI to treat the medium contaminated by the
515 residual DNAPL left in the LPL and the results are shown in figure S5. Here, the NZVI-suspensions
516 were not dispersed before injection. Yet, this did not affect the overall behaviors of the injected
517 fluids.

518 The initial step of the first strategy was the X2SD treatment. Then, the NZVI-xanthan solution was
519 injected in the LPL. The NZVI flowed preferentially upwards into the HPL because of the lower
520 hydraulic resistance. Nevertheless, the NZVI propagated along the HPL/LPL interface since the
521 injection of xanthan (blue color) was maintained in the HPL and acted as a downward force. This
522 result is interesting since it allowed the creation of a permeable reactive NZVI-barrier protecting
523 groundwater from COHs diffusion from the contaminated LPL, limiting rebound effect that is likely to
524 happen from low to high permeability strata [84].

525 In the second strategy, the HPL was first blocked with polymer foams (xanthan 2 g.l^{-1} + SDBS
526 $1.3 \times \text{CMC}$). Polymer was added to the formulation to generate stronger foams with better stability
527 and blocking capability and as previously reported [72,85–87]. 94% of the DNAPL was then recovered
528 after the injection of X2S in the LPL. Finally, the xanthan-NZVI solution was injected in the LPL.
529 Contrary to the first strategy, the NZVI remained only in the LPL without upward migration. The

530 absence of NZVI in the HPL stemmed from an inversion in the permeabilities. In this case, this
531 resulted from the effective blocking property of the viscous foam. For both strategies, the NZVI
532 concentration decreased with the distance in the LPL, as previously observed from the columns
533 experiments and reported by many [10,80,83].

534 To summarize, both strategies are viable and can be designed for field-scale. However, the first
535 strategy is simpler. It is also technically more feasible, as it requires fewer injection steps parameters
536 to control, especially during the foam injection step.

537

538 5. Conclusions

539 The pure phase recovery of a COH-DNAPL from a model aquifer made of a permeability-contrasted
540 bilayer overhanging an egg-box shaped substratum was studied. Benefits of viscosifying and tension-
541 active effects without density modification were assessed for different aqueous fluids from pure
542 water to xanthan solutions and surfactant foams. DNAPL-recovery increased by 2.1 and 3.3-times as
543 compared to pure water from tension-active and viscosity effects, respectively. When combined in a
544 flushing fluid made of xanthan 2 g.l⁻¹ and SDBS 1.3×CMC, the pure phase recovery was improved by a
545 4.2 factor and reached approximately 90% in 2D-experiments. It was observed that polymer solutions
546 are more controllable and robust than foams as flushing fluids. STR and NSTR were compared and
547 provided similar recovery rates for the best chemical formulations of the displacing fluids, yet the
548 former allowed to reduce the xanthan concentration by a factor of 10 to 20. In addition, it is
549 anticipated that STR should be more robust to face 3D-systems. Whenever possible and regardless of
550 DNAPL-recovery or NZVI-delivery, the high permeability layer should be blocked first before flushing
551 to improve the sweeping efficiency at high to low permeability interfaces and of the LPL where
552 DNAPL accumulates. This shear-thinning polymer technology is therefore promising for the *in situ*
553 remediation of anisotropic soils contaminated with DNAPLs. Nevertheless, a detailed hydrogeological
554 site characterization is crucial to strongly reduce the risks of uncontrolled pollutant mobilization and
555 uncertainties during rehabilitation operations.

556 6. Acknowledgements

557 This work was carried out as a part of the PAPIRUS project funded by the French Environmental
558 Agency (ADEME). Laura Fatin-Rouge is acknowledged for her help to improve the English of the
559 manuscript.

560 7. References

- 561 [1] Z.L. Hildenbrand, D.D. Carlton, B.E. Fontenot, J.M. Meik, J.L. Walton, J.T. Taylor, J.B. Thacker,
562 S. Korlie, C.P. Shelor, D. Henderson, A.F. Kadjo, C.E. Roelke, P.F. Hudak, T. Burton, H.S. Rifai,
563 K.A. Schug, A Comprehensive Analysis of Groundwater Quality in The Barnett Shale Region,
564 *Environ. Sci. Technol.* 49 (2015) 8254–8262. doi:10.1021/acs.est.5b01526.
- 565 [2] Z.L. Hildenbrand, D.D. Carlton, B.E. Fontenot, J.M. Meik, J.L. Walton, J.B. Thacker, S. Korlie,
566 C.P. Shelor, A.F. Kadjo, A. Clark, S. Usenko, J.S. Hamilton, P.M. Mach, G.F. Verbeck, P. Hudak,
567 K.A. Schug, Temporal variation in groundwater quality in the Permian Basin of Texas, a region
568 of increasing unconventional oil and gas development, *Sci. Total Environ.* 562 (2016) 906–913.
569 doi:10.1016/j.scitotenv.2016.04.144.
- 570 [3] E.L. DiFilippo, M.L. Brusseau, Relationship between mass-flux reduction and source-zone mass
571 removal: Analysis of field data, *J. Contam. Hydrol.* 98 (2008) 22–35.
572 doi:10.1016/j.jconhyd.2008.02.004.
- 573 [4] J. Maire, A. Coyer, N. Fatin-rouge, Surfactant foam technology for in situ removal of heavy
574 chlorinated, *J. Hazard. Mater.* 299 (2015) 630–638. doi:10.1016/j.jhazmat.2015.07.071.
- 575 [5] Interstate Technology & Regulatory Council, 2002. <https://www.itrcweb.org>.
- 576 [6] K.M. Rathfelder, L.M. Abriola, M.A. Singletary, K.D. Pennell, Influence of surfactant-facilitated
577 interfacial tension reduction on chlorinated solvent migration in porous media: Observations
578 and numerical simulation, *J. Contam. Hydrol.* 64 (2003) 227–252. doi:10.1016/S0169-
579 7722(02)00205-X.
- 580 [7] T. Robert, R. Martel, S.H. Conrad, R. Lefebvre, U. Gabriel, Visualization of TCE recovery
581 mechanisms using surfactant-polymer solutions in a two-dimensional heterogeneous sand
582 model, *J. Contam. Hydrol.* 86 (2006) 3–31. doi:10.1016/j.jconhyd.2006.02.013.
- 583 [8] I. Bouzid, J. Maire, F. Laurent, M. Broquaire, N. Fatin-Rouge, Controlled treatment of a high
584 velocity anisotropic aquifer model contaminated by hexachlorocyclohexanes, *Environ. Pollut.*
585 268 (2021) 115678. doi:10.1016/j.envpol.2020.115678.
- 586 [9] I. Bouzid, D. Pino Herrera, M. Dierick, Y. Pechaud, V. Langlois, P.-Y. Klein, J. Albaric, N. Fatin-
587 Rouge, A new foam-based method for the (bio)degradation of hydrocarbons in contaminated
588 vadose zone, *J. Hazard. Mater.* 401 (2021) 123420. doi:10.1016/j.jhazmat.2020.123420.
- 589 [10] Y. Su, Y. Zhao, L. Li, C. Qin, Enhanced Delivery of Nanoscale Zero-Valent Iron in Porous Media
590 by Sodium Dodecyl Sulfate Solution and Foam, *Environ. Eng. Sci.* 32 (2015) 684–693.

- 591 doi:10.1089/ees.2014.0529.
- 592 [11] R. Lenormand, E. Touboul, C. Zarcone, Numerical models and experiments on immiscible
593 displacements in porous media, *J. Fluid Mech.* 189 (1988) 165–187.
594 doi:10.1017/S0022112088000953.
- 595 [12] L.W. Lake, *Enhanced oil recovery.*, Prentice Hall Englewood Cliffs, NJ, 1989.
- 596 [13] A. Muggeridge, A. Cockin, K. Webb, H. Frampton, I. Collins, T. Moulds, P. Salino, Recovery
597 rates, enhanced oil recovery and technological limits, *Philos. Trans. R. Soc. A Math. Phys. Eng.*
598 *Sci.* 372 (2014). doi:10.1098/rsta.2012.0320.
- 599 [14] D.A.Z. Wever, F. Picchioni, A.. Broekhuis, Polymers for enhanced oil recovery: A paradigm for
600 structure–property relationship in aqueous solution, *Prog. Polym. Sci.* 36 (2011) 1558–1628.
- 601 [15] X. Xu, A. Saeedi, Evaluation and Optimization Study on a Hybrid EOR Technique Named as
602 Chemical-Alternating-Foam Floods, *Oil Gas Sci. Technol.* 72 (2017) 1–14.
603 doi:10.2516/ogst/2016022.
- 604 [16] C. Wei, J. Zheng, L. Xiong, Z. Li, J. Yang, J. Zhang, S. Lin, L. Zhou, L. Fang, Y. Ding, Evaluation and
605 utilization of nano-micron polymer plug for heterogeneous carbonate reservoir with thief
606 zones, *Adv. Polym. Technol.* 2020 (2020). doi:10.1155/2020/3498583.
- 607 [17] K.S. Sorbie, R.S. Seright, P. Recovery, Gel Placement in Heterogeneous Systems With
608 Crossflow, in: *SPE, Society of Petroleum Engineers, Tulsa, Oklahoma, 1992: p. 369.*
609 doi:https://doi.org/10.2118/24192-MS.
- 610 [18] I. Bouzid, J. Maire, S.I. Ahmed, N. Fatin-Rouge, Enhanced remedial reagents delivery in
611 unsaturated anisotropic soils using surfactant foam, *Chemosphere.* 210 (2018).
612 doi:10.1016/j.chemosphere.2018.07.081.
- 613 [19] I. Bouzid, J. Maire, N. Fatin-Rouge, Comparative assessment of a foam-based oxidative
614 treatment of hydrocarbon-contaminated unsaturated and anisotropic soils, *Chemosphere.*
615 233 (2019). doi:10.1016/j.chemosphere.2019.05.295.
- 616 [20] F. Gastone, T. Tosco, R. Sethi, Guar gum solutions for improved delivery of iron particles in
617 porous media (Part 1): Porous medium rheology and guar gum-induced clogging, *J. Contam.*
618 *Hydrol.* 166 (2014) 23–33. doi:10.1016/j.jconhyd.2014.06.013.
- 619 [21] L. Zhong, M. Oostrom, M.J. Truex, V.R. Vermeul, J.E. Szecsody, Rheological behavior of
620 xanthan gum solution related to shear thinning fluid delivery for subsurface remediation, *J.*

- 621 Hazard. Mater. 244–245 (2013) 160–170. doi:10.1016/j.jhazmat.2012.11.028.
- 622 [22] J. Xin, F. Tang, X. Zheng, H. Shao, O. Kolditz, Transport and retention of xanthan gum-
623 stabilized microscale zero-valent iron particles in saturated porous media, *Water Res.* 88
624 (2016) 199–206. doi:10.1016/j.watres.2015.10.005.
- 625 [23] S.C. Hauswirth, P.S. Birak, S.C. Rylander, C.T. Miller, Mobilization of manufactured gas plant
626 tar with alkaline flushing solutions, *Environ. Sci. Technol.* 46 (2012) 426–433.
627 doi:10.1021/es202278s.
- 628 [24] I. Bouzid, J. Maire, N. Fatin-rouge, Comparative assessment of a foam-based method for ISCO
629 of coal tar contaminated unsaturated soils, *J. Environ. Chem. Eng.* 7 (2019) 103346.
630 doi:10.1016/j.jece.2019.103346.
- 631 [25] J. Maire, A. Joubert, D. Kaifas, T. Invernizzi, J. Marduel, S. Colombano, D. Cazaux, C. Marion, P.
632 Klein, A. Dumestre, N. Fatin-rouge, Assessment of flushing methods for the removal of heavy
633 chlorinated compounds DNAPL in an alluvial aquifer, *Sci. Total Environ.* 612 (2018) 1149–
634 1158. doi:10.1016/j.scitotenv.2017.08.309.
- 635 [26] J. Maire, N. Fatin-Rouge, Surfactant foam flushing for in situ removal of DNAPLs in shallow
636 soils, *J. Hazard. Mater.* 321 (2017) 247–255. doi:10.1016/j.jhazmat.2016.09.017.
- 637 [27] S. Comba, D. Dalmazzo, E. Santagata, R. Sethi, Rheological characterization of xanthan
638 suspensions of nanoscale iron for injection in porous media, *J. Hazard. Mater.* 185 (2011)
639 598–605. doi:10.1016/j.jhazmat.2010.09.060.
- 640 [28] R. Martel, R. Lefebvre, P.J. Gélinas, Aquifer washing by micellar solutions: 2. DNAPL recovery
641 mechanisms for an optimized alcohol-surfactant-solvent solution, *J. Contam. Hydrol.* 30
642 (1998) 1–31. doi:10.1016/S0169-7722(97)00030-2.
- 643 [29] C. Portois, E. Essouayed, M.D. Annable, N. Guiserix, A. Joubert, O. Atteia, Field demonstration
644 of foam injection to confine a chlorinated solvent source zone, *J. Contam. Hydrol.* 214 (2018)
645 16–23. doi:10.1016/j.jconhyd.2018.04.003.
- 646 [30] S.W. Jeong, Evaluation of the use of capillary numbers for quantifying the removal of DNAPL
647 trapped in a porous medium by surfactant and surfactant foam floods, *J. Colloid Interface Sci.*
648 282 (2005) 182–187. doi:10.1016/j.jcis.2004.08.108.
- 649 [31] S.W. Giese, S.E. Powers, Using polymer solutions to enhance recovery of mobile coal tar and
650 creosote DNAPLs, *J. Contam. Hydrol.* 58 (2002) 147–167. doi:10.1016/S0169-7722(02)00009-

- 651 8.
- 652 [32] G.J. Hirasaki, C.A. Miller, R. Szafranski, D. Tanzil, J.B. Lawson, H. Meinardus, M. Jin, J.T.
653 Londergan, R.E. Jackson, G.A. Pope, W.H. Wade, Field Demonstration of the Surfactant/Foam
654 Process for Aquifer Remediation, in: SPE Annu. Tech. Conf. Exhib., Society of Petroleum
655 Engineers, 5-8 October, San Antonio, Texas, 1997.
- 656 [33] R. Szafranski, J. Lawson, G. Hirasaki, C. Miller, N. Akiya, S. King, R. Jackson, H. Meinardus, J.
657 Londergan, Surfactant/foam process for improved efficiency of aquifer remediation, *Struct.*
658 *Dyn. Prop. Disperse Colloid. Syst.* 111 (1998) 162–167.
- 659 [34] R. Martel, A. Hébert, R. Lefebvre, P. Gélinas, U. Gabriel, Displacement and sweep efficiencies
660 in a DNAPL recovery test using micellar and polymer solutions injected in a five-spot pattern,
661 *J. Contam. Hydrol.* 75 (2004) 1–29. doi:10.1016/j.jconhyd.2004.03.007.
- 662 [35] R. Martel, P.J. Gélinas, L. Saumure, Aquifer washing by micellar solutions: 3 field test at the
663 Thouin Sand Pit (L'Assomption, Quebec, Canada), *J. Contam. Hydrol.* 30 (1998) 33–48.
664 doi:10.1016/S0169-7722(97)00031-4.
- 665 [36] C.M. Dominguez, S. Rodriguez, D. Lorenzo, A. Romero, A. Santos, Degradation of
666 Hexachlorocyclohexanes (HCHs) by Stable Zero Valent Iron (ZVI) Microparticles, *Water. Air.*
667 *Soil Pollut.* 227 (2016). doi:10.1007/s11270-016-3149-8.
- 668 [37] X. Li, L. Liu, Recent advances in nanoscale zero-valent iron/oxidant system as a treatment for
669 contaminated water and soil, *J. Environ. Chem. Eng.* 9 (2021).
670 doi:10.1016/j.jece.2021.106276.
- 671 [38] Q. Li, Z. Chen, H. Wang, H. Yang, T. Wen, S. Wang, B. Hu, X. Wang, Removal of organic
672 compounds by nanoscale zero-valent iron and its composites, *Sci. Total Environ.* 792 (2021)
673 148546. doi:10.1016/j.scitotenv.2021.148546.
- 674 [39] L. Qian, Y. Chen, D. Ouyang, W. Zhang, L. Han, J. Yan, P. Kvpil, M. Chen, Field demonstration
675 of enhanced removal of chlorinated solvents in groundwater using biochar-supported
676 nanoscale zero-valent iron, *Sci. Total Environ.* 698 (2020) 134215.
677 doi:10.1016/j.scitotenv.2019.134215.
- 678 [40] J.Y. Ahn, C. Kim, S.C. Jun, I. Hwang, Field-scale investigation of nanoscale zero-valent iron
679 (NZVI) injection parameters for enhanced delivery of NZVI particles to groundwater, *Water*
680 *Res.* 202 (2021) 117402. doi:10.1016/j.watres.2021.117402.

- 681 [41] Q. Giraud, J. Gonçalves, B. Paris, A. Joubert, S. Colombano, D. Cazaux, 3D numerical modelling
682 of a pulsed pumping process of a large DNAPL pool: In situ pilot-scale case study of
683 hexachlorobutadiene in a keyed enclosure, *J. Contam. Hydrol.* 214 (2018) 24–38.
684 doi:10.1016/j.jconhyd.2018.05.005.
- 685 [42] L. Yung, J. Lagron, D. Cazaux, M. Limmer, M. Chalot, Phytoscreening as an efficient tool to
686 delineate chlorinated solvent sources at a chlor-alkali facility, *Chemosphere.* 174 (2017) 82–
687 89. doi:10.1016/j.chemosphere.2017.01.112.
- 688 [43] C. Tropea, A. Yarin, J.F. Foss, *Springer Handbook of Experimental Fluid Mechanics*, Springer
689 Science & Business Media, 2007.
- 690 [44] M.D. Murray, B.W. Darvell, A protocol for contact angle measurement, *J. Phys. D. Appl. Phys.*
691 23 (1990) 1150–1155. doi:10.1088/0022-3727/23/9/003.
- 692 [45] J. Bachmann, R. Horton, R.. Van Der Ploeg, S. Woche, Modified Sessile Drop Method for
693 assessing initial soil-water contact angle of sandy soil, *Soil. Sci. Soc. Am. J.* 64 (2000) 546–567.
- 694 [46] C. Igathinathane, L.O. Pordesimo, A.R. Womac, V.K. Malleswar, U.A. Rao, Viscosity
695 measurement technique using standard glass burette for newtonian liquids, *Instrum. Sci.*
696 *Technol.* 33 (2005) 101–125. doi:10.1081/CI-200040881.
- 697 [47] US EPA, *Multi-Phase Extraction: State-of-the-Practice*, 1999.
- 698 [48] S. Colombano, H. Davarzani, E. D. van Hullebusch, I. Ignatiadis, S. Huguenot, David Omirbekov,
699 D. Guyonnet, Free Product Recovery of Non-aqueous Phase Liquids in Contaminated Sites:
700 Theory and Case Studies, in: *Environ. Soil Remediat. Rehabil.*, Springer Nature, Switzerland,
701 2020: pp. 64–148. doi:https://doi.org/10.1007/978-3-030-40348-5_2.
- 702 [49] J. Maire, E. Brunol, N. Fatin-Rouge, Shear-thinning fluids for gravity and anisotropy mitigation
703 during soil remediation in the vadose zone, *Chemosphere.* 197 (2018) 661–669.
704 doi:10.1016/j.chemosphere.2018.01.101.
- 705 [50] S. Pandey, R.P. Bagwe, D.O. Shah, Effect of counterions on surface and foaming properties of
706 dodecyl sulfate, *J. Colloid Interface Sci.* 267 (2003) 160–166. doi:10.1016/j.jcis.2003.06.001.
- 707 [51] US EPA, *Hydraulic fracturing technology*, EPA 540-R-93-505. (1993) 140.
- 708 [52] A.M. Zafar, M.A. Javed, A.A. Hassan, M.M. Mohamed, Groundwater remediation using zero-
709 valent iron nanoparticles (nZVI), *Groundw. Sustain. Dev.* 15 (2021) 100694.
710 doi:10.1016/j.gsd.2021.100694.

- 711 [53] A. Tiraferri, K.L. Chen, R. Sethi, M. Elimelech, Reduced aggregation and sedimentation of zero-
712 valent iron nanoparticles in the presence of guar gum, *J. Colloid Interface Sci.* 324 (2008) 71–
713 79. doi:10.1016/j.jcis.2008.04.064.
- 714 [54] R. Duan, Y. Dong, Q. Zhang, Characteristics of aggregate size distribution of nanoscale zero-
715 valent iron in aqueous suspensions and its effect on transport process in porous media, *Water*
716 (Switzerland). 10 (2018). doi:10.3390/w10060670.
- 717 [55] A. Ogata, R.B. Banks, A solution of the differential equation of longitudinal dispersion in
718 porous media, *Geol. Surv. (U.S.); Prof. Pap.* (1961) A1–A7.
719 <http://pubs.er.usgs.gov/publication/pp411A>.
- 720 [56] J.T. Woods, M.G. Mellon, Thiocyanate Method for Iron A Spectrophotometric Study, *Ind. Eng.*
721 *Chem. - Anal. Ed.* 13 (1941) 551–554. doi:10.1021/i560096a013.
- 722 [57] K.D. Pennell, G.A. Pope, L.M. Abriola, Influence of viscous and buoyancy forces on the
723 mobilization of residual tetrachloroethylene during surfactant flushing, *Environ. Sci. Technol.*
724 30 (1996) 1328–1335. doi:10.1021/es9505311.
- 725 [58] Y. Li, L.M. Abriola, T.J. Phelan, C.A. Ramsburg, K.D. Pennell, Experimental and numerical
726 validation of the total trapping number for prediction of DNAPL mobilization, *Environ. Sci.*
727 *Technol.* 41 (2007) 8135–8141. doi:10.1021/es070834i.
- 728 [59] S.G. Huling, J.W. Weaver, Ground water issue: Dense nonaqueous phase liquids, United States
729 *Environ. Prot. Agency.* (1992) 1–25. doi:10.1056/NEJMoa030660.
- 730 [60] B.H. Kueper, G.P. Wealhall, J.W.N. Smith, S. a Leharne, D.N. Lerner, An illustrated handbook
731 of DNAPL transport and fate in the subsurface, 2003. www.environment-agency.gov.uk.
- 732 [61] Y. Yao, M. Wei, W. Kang, A review of wettability alteration using surfactants in carbonate
733 reservoirs, *Adv. Colloid Interface Sci.* 294 (2021) 102477. doi:10.1016/j.jcis.2021.102477.
- 734 [62] S. Ayirala, A. Sofi, Z. Li, Z. Xu, Surfactant and surfactant-polymer effects on wettability and
735 crude oil liberation in carbonates, *J. Pet. Sci. Eng.* 207 (2021) 109117.
736 doi:10.1016/j.petrol.2021.109117.
- 737 [63] L. Li, J. Chen, X. Jin, Z. Wang, Y. Wu, C. Dai, Novel polyhydroxy anionic surfactants with
738 excellent water-solid interfacial wettability control capability for enhanced oil recovery, *J.*
739 *Mol. Liq.* 343 (2021) 116973. doi:10.1016/j.molliq.2021.116973.
- 740 [64] N. Yekeen, E. Padmanabhan, A.H. Syed, T. Sevo, K. Kanesen, Synergistic influence of

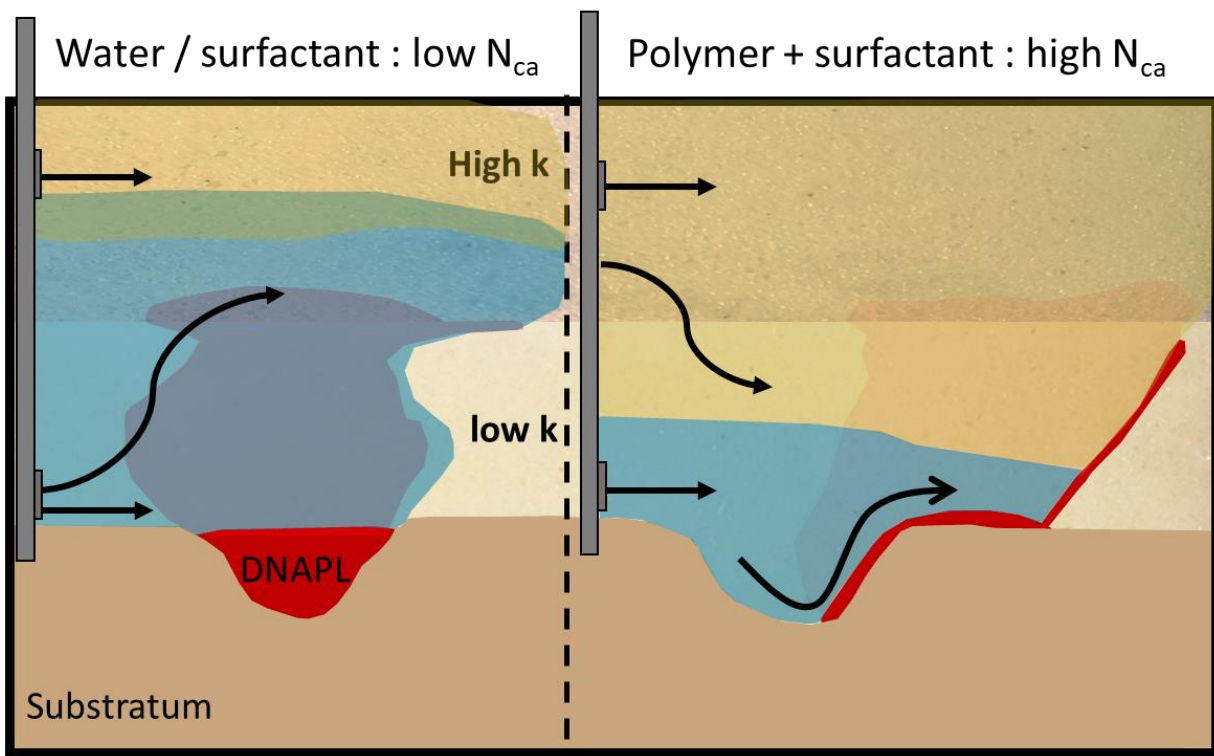
- 741 nanoparticles and surfactants on interfacial tension reduction, wettability alteration and
742 stabilization of oil-in-water emulsion, *J. Pet. Sci. Eng.* 186 (2020) 106779.
743 doi:10.1016/j.petrol.2019.106779.
- 744 [65] J. Lian, Y. Fu, C. Guo, Y. He, C. Qin, Performance of polymer-enhanced KMnO₄ delivery for
745 remediation of TCE contaminated heterogeneous aquifer: A bench-scale visualization, *J.*
746 *Contam. Hydrol.* 225 (2019). doi:10.1016/j.jconhyd.2019.103507.
- 747 [66] L. Ren, R. Wang, B. Qin, D. Liu, J. Sang, J. Dong, Enhanced remediation efficiency of Cr(VI)-
748 contaminated heterogeneous aquifers: Improved sweeping efficiency using shear-thinning
749 fluids, *Chemosphere.* 273 (2021). doi:10.1016/j.chemosphere.2021.129675.
- 750 [67] M. Simjoo, T. Rezaei, A. Andrianov, P.L.J.J. Zitha, Foam stability in the presence of oil: Effect of
751 surfactant concentration and oil type, *Colloids Surfaces A Physicochem. Eng. Asp.* 438 (2013)
752 148–158. doi:10.1016/j.colsurfa.2013.05.062.
- 753 [68] G.J. Hirasaki, C.A. Miller, R. Szafranski, J.B. Lawson, N. Akiya, Surfactant/foam process for
754 aquifer remediation, *Proc. - SPE Int. Symp. Oilf. Chem.* (1997) 471–480. doi:10.2523/37257-
755 ms.
- 756 [69] H.J. Bertin, O.G. Apaydin, L.M. Castanier, A.R. Kovscek, U. Stanford, Foam Flow in
757 Heterogeneous Porous Media : Effect of Cross Flow, *SPE J.* 4 (1999) 75–82.
758 doi:10.2118/56009-PA.
- 759 [70] F. Casteel, C.S. Oil, G. Corp, Sweep Improvement in CO₂ Flooding by Use of Foaming Agents,
760 *SPE Reserv. Eng.* 3 (1988). doi:https://doi.org/10.2118/14392-PA.
- 761 [71] I. Bouzid, J. Maire, N. Fatin-Rouge, Comparative assessment of a foam-based oxidative
762 treatment of hydrocarbon-contaminated unsaturated and anisotropic soils, *Chemosphere.*
763 233 (2019) 667–676. doi:10.1016/j.chemosphere.2019.05.295.
- 764 [72] N. Forey, O. Atteia, A. Omari, H. Bertin, Saponin foam for soil remediation: On the use of
765 polymer or solid particles to enhance foam resistance against oil, *J. Contam. Hydrol.* (2019)
766 103560. doi:10.1016/j.jconhyd.2019.103560.
- 767 [73] J. Maire, H. Davarzani, S. Colombano, N. Fatin-Rouge, Targeted delivery of hydrogen for the
768 bioremediation of aquifers contaminated by dissolved chlorinated compounds, *Environ.*
769 *Pollut.* 249 (2019) 443–452. doi:10.1016/j.envpol.2019.03.033.
- 770 [74] S. Liao, Z. Saleeba, J.D. Bryant, L.M. Abriola, K.D. Pennell, Influence of aqueous film forming

- 771 foams on the solubility and mobilization of non-aqueous phase liquid contaminants in quartz
772 sands, *Water Res.* 195 (2021) 116975. doi:10.1016/j.watres.2021.116975.
- 773 [75] B.L. Longino, B.H. Kueper, Effects of capillary pressure and use of polymer solutions on dense,
774 non-aqueous-phase liquid retention and mobilization in a rough-walled fracture, *Environ. Sci.*
775 *Technol.* 33 (1999) 2447–2455. doi:10.1021/es980752h.
- 776 [76] S.S. Suthersan, J. McDonough, *Remediation Engineering: Design Concepts*, Lewis Publishers,
777 Boca Raton, FL, 1996.
- 778 [77] E. Dalla Vecchia, M. Luna, R. Sethi, Transport in porous media of highly concentrated iron
779 micro- and nanoparticles in the presence of xanthan gum, *Environ. Sci. Technol.* 43 (2009)
780 8942–8947. doi:10.1021/es901897d.
- 781 [78] H.M. Ibrahim, M. Awad, A.S. Al-Farraj, A.M. Al-Turki, Effect of flow rate and particle
782 concentration on the transport and deposition of bare and stabilized zero-valent iron
783 nanoparticles in sandy soil, *Sustain.* 11 (2019) 1–13. doi:10.3390/su11236608.
- 784 [79] A. Mondal, B.K. Dubey, M. Arora, K. Mumford, Porous media transport of iron nanoparticles
785 for site remediation application: A review of lab scale column study, transport modelling and
786 field-scale application, *J. Hazard. Mater.* 403 (2021). doi:10.1016/j.jhazmat.2020.123443.
- 787 [80] J. Li, S. Ghoshal, Comparison of the transport of the aggregates of nanoscale zerovalent iron
788 under vertical and horizontal flow, *Chemosphere.* 144 (2016) 1398–1407.
789 doi:10.1016/j.chemosphere.2015.09.103.
- 790 [81] S. Xu, B. Gao, J.E. Saiers, Straining of colloidal particles in saturated porous media, *Water*
791 *Resour. Res.* 42 (2006) 1–10. doi:10.1029/2006WR004948.
- 792 [82] L. Chekli, G. Brunetti, E.R. Marzouk, A. Maoz-Shen, E. Smith, R. Naidu, H.K. Shon, E. Lombi, E.
793 Donner, Evaluating the mobility of polymer-stabilised zero-valent iron nanoparticles and their
794 potential to co-transport contaminants in intact soil cores, *Environ. Pollut.* 216 (2016) 636–
795 645. doi:10.1016/j.envpol.2016.06.025.
- 796 [83] T.J. Strutz, G. Hornbruch, A. Dahmke, R. Köber, Influence of permeability on nanoscale zero-
797 valent iron particle transport in saturated homogeneous and heterogeneous porous media,
798 *Environ. Sci. Pollut. Res.* 23 (2016) 17200–17209. doi:10.1007/s11356-016-6814-y.
- 799 [84] D. O'Connor, D. Hou, Y.S. Ok, Y. Song, A.K. Sarmah, X. Li, F.M.G. Tack, Sustainable in situ
800 remediation of recalcitrant organic pollutants in groundwater with controlled release

- 801 materials: A review, *J. Control. Release.* 283 (2018) 200–213.
802 doi:10.1016/j.jconrel.2018.06.007.
- 803 [85] R. Petkova, S. Tcholakova, N.D. Denkov, Foaming and foam stability for mixed polymer-
804 surfactant solutions: Effects of surfactant type and polymer charge, *Langmuir.* 28 (2012)
805 4996–5009. doi:10.1021/la3003096.
- 806 [86] A. Telmadarreie, J. Trivedi, Static and Dynamic Performance of Wet Foam and Polymer-
807 Enhanced Foam in the Presence of Heavy Oil, *Colloids and Interfaces.* 2 (2018) 38.
808 doi:10.3390/colloids2030038.
- 809 [87] G. Jian, Q. Hou, Y. Zhu, Stability of Polymer and Surfactant Mixture Enhanced Foams in the
810 Presence of Oil Under Static and Dynamic Conditions, *J. Dispers. Sci. Technol.* 36 (2015) 477–
811 488. doi:10.1080/01932691.2014.907539.

812

① DNAPL recovery



20—40 % recovery

88—93 % recovery

② NZVI delivery

